BMC Chemistry

RESEARCH Open Access

Changes in the state of matter of $KClO_4$ to improve thermal and combustion properties of Al/MoO_3 nanothermite

Jialin Chen[1†], Shutao Li[1†], Mengnan Dai[1†], Ming An[2], Rui Song[3], Yeqing Chen[1], Jiaxing Song[4], Quanwei Tian[4], Xiting Zhong[4] and Qiushi Yan[5*]

Abstract

To improve the thermal and combustion properties of nanothermites, a design theory of changing the state of matter and structural state of the reactants during reaction was proposed. The Al/MoO_3/$KClO_4$ (Kp) nanothermite was prepared and the Al/MoO_3 nanothermite was used as a control. SEM and XRD were used to characterize the nanothermites; DSC was used to test thermal properties; and constant volume and open combustion tests were performed to examine their combustion performance. Phase and morphology characterization of the combustion products were performed to reveal the mechanism of the aluminothermic reaction. The results show that the Al/MoO_3/Kp nanothermite exhibited excellent thermal properties, with a total heat release of 1976 J·g^{-1}, increasing by approximately 33% of 1486 J·g^{-1} of the Al/MoO_3 nanothermite, and activation energy of 269.66 kJ·mol^{-1}, which demonstrated higher stability than the Al/MoO_3 nanothermite (205.64 kJ·mol^{-1}). During the combustion test, the peak pressure of the Al/MoO_3/Kp nanothermite was 0.751 MPa, and the average pressure rise rate was 25.03 MPa·s^{-1}, much higher than 0.188 MPa and 6.27 MPa·s^{-1} of the Al/MoO_3 nanothermite. The combustion products of Al/MoO_3 nanothermite were Al_2O_3, MoO, and Mo, indicating insufficient combustion and incomplete reaction, whereas, the combustion products of Al/MoO_3/Kp nanothermite were Al_2O_3, MoO, and KCl, indicating complete reaction. Their "coral-like" morphology was the effect of reactants solidifying after melting during the combustion process. The characterization of reactants and pressure test during combustion reveals the three stages of aluminothermic reaction in thermites. The excellent thermal and combustion performance of Al/MoO_3/Kp nanothermite is attributed to the melt and decomposition of Kp into O_2 in the third stage. This study provides new ideas and guidance for the design of high-performance nanothermites.

Keywords Thermite, Constant volume combustion, Melt and decomposition, Thermodynamics analysis

†Jialin Chen, Shutao Li, Mengnan Dai equal first contribution to this work.

*Correspondence:
Qiushi Yan
yqs2011@bjut.edu.cn
[1]Institute of Defense Engineering, AMS, PLA, Beijing, China
[2]School of Physics, Southeast University, Nanjing, China
[3]Department of General Education, Army Engineering University of PLA, Nanjing, China
[4]Xi'an Rare Metal Materials Research Institute Co., Ltd, Xi'an, China
[5]Key Laboratory of Urban Security and Disaster Engineering under the Ministry of Education, Beijing University of Technology, Beijing, China

Introduction

Nanothermite, a nanoscale fuel and oxidizer particle mixture, has a shorter diffusion distance than conventional micron-sized or monomolecular energetic materials. Therefore, it has a very high energy release rate, which releases a large amount of heat, demonstrating good combustion and thermal properties [1–6].

Currently, there are extensive published findings on oxidizers such as Al/MoO_3, Al/NiO, Al/SiO_2, Al/WO_3, Al/CuO thermites, etc [7–13]. . . . Among numerous oxides, MoO_3 has unique chemical and physical properties for applications in the fields of optics, electronics, catalysis, biology, energy systems [14–17], etc. More importantly, it holds an advantage in the application of thermites. Stoichiometric ratio calculation implies that the exothermic enthalpy of MoO_3 is higher than most metal oxides. Research has shown that Al/MoO_3 nanothermite has better ignition performance [14], therefore, as an oxide in thermites, more potentials of MoO_3 remain to be investigated. Thanks to its high heat, high redox potential, and rapid reactivity [18, 19], nano Al has been used as the main constituent of solid rocket propellants and other propulsion systems [18]. However, Al nanoparticles are prone to agglomeration adhesion [20], which has a great impact on the process of aluminothermic reaction. The sintering products from local precombustion may block the combustion progress [21, 22], and hinder the self-propagating combustion of thermite, keeping heat from complete release.

Therefore, maintaining a good dispersion of nano Al or designing a novel structure with a large interface contact area can greatly improve the reactivity of fuel with the oxidant. To increase the contact area of reactants, various preparation methods and strategies have been investigated, such as sol-gel synthesis [23], vapor deposition [24], self-assembly [3], high-energy ball milling [25], etc. A variety of thermite structures have been prepared, including 3D-ordered array nanothermite film [26], core-shell structures [27], etc. Novel preparation methods and structures can effectively improve combustion characteristics and greatly increase safety yet with the disadvantages of cumbersome operation techniques and high preparation costs.

The foregoing studies aimed to increase interfacial reactions by modulating the initial structure of reactants, thereby improving the thermal and combustion properties. However, is it possible to use the structural changes in reaction to increase the contact area? For this purpose, a nanothermite that produces gas and undergoes changes in the state of matter during the reaction can be designed. The addition of gas-producing agents is an outstanding method. The agents generate gases during the reaction, thus increasing the pressure in the reaction system, prompting closer contact at the reaction interfaces and increasing the overall reactivity, e.g., nitrocellulose (NC) [28], copper oxide (CuO) [29], bismuth oxide (Bi_2O_3) [30], etc. In terms of the reactant states, most of the current thermites undergo a solid-solid reaction during the aluminothermic reaction [31, 32], whereas few studies have been reported on the changes in the state of matter during the main reaction.

Potassium perchlorate ($KClO_4$, Kp) is an excellent additive that decomposes into O_2 under high-temperature conditions, which has a melting temperature close to the reaction temperature of nanothermites. Therefore, it has been shown that as an excellent additive, it can substantially improve the combustion performance of thermites [33, 34]. However, until recently, there have been few studies on the mechanism of why it can promote the reaction of thermites, and the specific reaction path has not yet been revealed. Further systematic exploration is still needed.

In this study, the hydrothermal method was used to prepare nano-MoO_3, and the ultrasonic dispersion method was used to prepare Al/MoO_3/Kp nanothermite. The prepared nanothermite was tested for thermal and combustion properties, and thermodynamics analysis was performed to calculate activation energy. The combustion products were collected to investigate the reaction state of the aluminothermic reaction process and the reaction mechanism of Al/MoO_3/Kp nanothermite. Moreover, Al/MoO_3 nanothermite was prepared for comparison.

Experiment

Material preparation

$(NH_4)_6Mo_7O_{24}{\cdot}4H_2O$ (99% purity) was provided by Shanghai Bide Pharmatech Ltd. $KClO_4$ (Kp) and nano Al powder were provided by Aladdin Industries. Dimethylformamide (DMF, 99.8%), anhydrous ethanol (99.7%), deionized water, and HNO_3 (concentration 68%) were provided by Sinopharm Chemical Reagent Co., Ltd. All reagents were used directly without any treatment.

Preparation of nano-MoO_3

Nano-MoO_3 was prepared using the hydrothermal method, and the preparation process is shown in Fig. 1(a). The early chemical reaction took place in an N_2 atmosphere. To ensure the smooth progress of the reaction, a suitable installation was set up using vessels such as flasks and constant pressure funnels. First, an ammonium molybdate solution was prepared using 1.5 g $(NH_4)_6Mo_7O_{24}{\cdot}4H_2O$ and 30 ml of deionized water, and magnetically stirred for 30 min at 40 °C in a water bath. Afterwards, the diluted HNO_3 solution was added drop by drop to the ammonium molybdate solution, and the chemical reaction was ensured to take place under the N_2 atmosphere. With the addition of the acid solution,

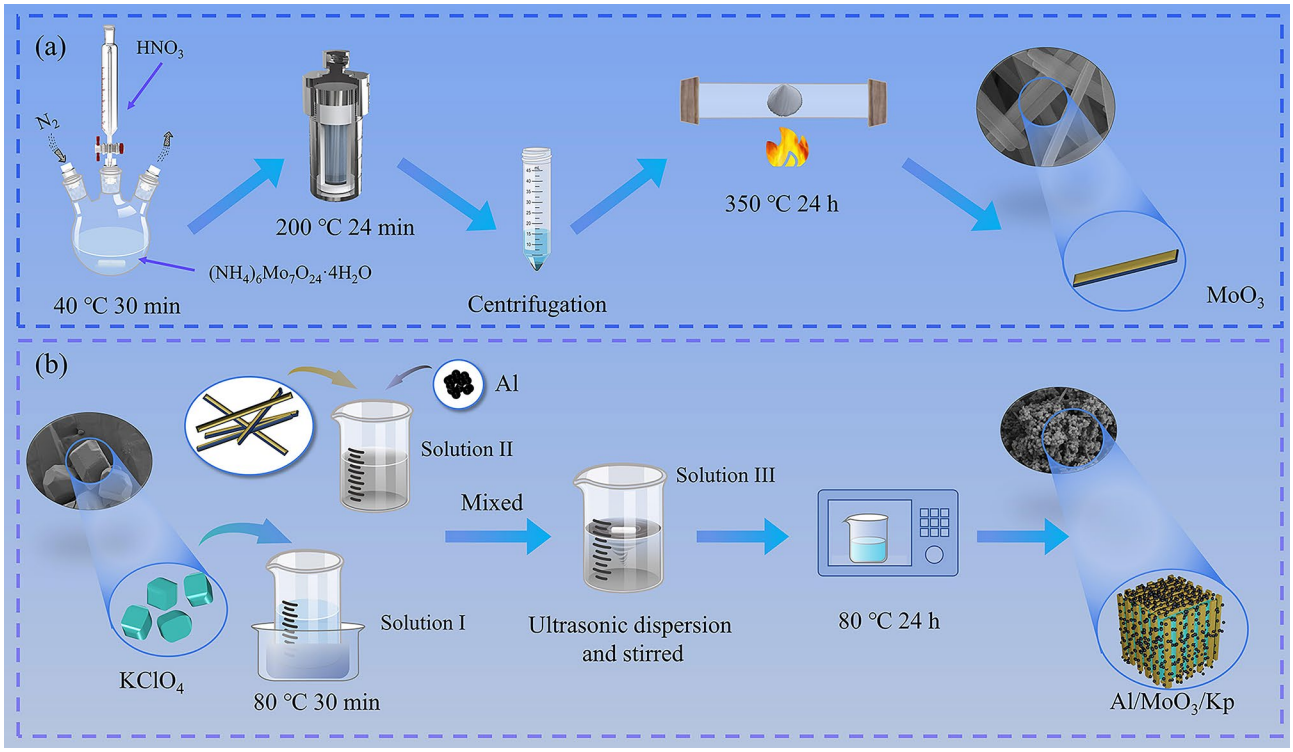

Fig. 1 Preparation flow chart (**a**) nano-MoO_3 preparation flow chart (**b**) nanothermite preparation flow chart

Table 1 Nanothermite oxidant and fuel ratio table

Sample	MoO_3/mg	$KClO_4$/mg	Al/mg
Al/MoO_3 nanothermite	120	0	69
Al/MoO_3/Kp nanothermite	75	45	79

the color of the solution changed from colorless to milky white and then to clear colorless. After the reaction was completed, the solution was moved to a high-pressure reactor lined with polytetrafluoroethylene, and heated at 200 °C for 24 h. Subsequently, the solution was washed three times with deionized water and centrifuged. The precipitates were dried and heated at 350 °C for 24 h before being ground to obtain the nano-MoO_3 sample. The main chemical reactions are shown in formula (1):

$$Mo_7O_{24}^{6-}+6H^+ \rightarrow 7MoO_3+3H_2O \quad (1)$$

Nanothermite preparation

Due to the existence of an oxide layer, the activity of the nano Al powder will not be 100% [35]. The activity of nano Al powder was measured before the preparation of nanothermite. To analyze the content of active Al, tests were conducted using a synchronous thermal analyzer (TG-DSC) at 30?~1200 °C, with a heating rate of 10 K·min^{-1} and an air flow rate of 50 ml·min^{-1} to ensure complete oxidation of the Al nanoparticles. The oxidation reaction of Al in air is shown in formula (2):

$$4Al + 3O_2 = 2Al_2O_3 \quad (2)$$

Figure 3(a) exhibits the TG-DSC profile of nano Al thermal analysis, which shows a significant increase in mass, reaching 158.22% of the original mass. The increase is attributed to the oxidation of active Al. Formula (3) can be used to calculate the content (c) of active Al:

$$c\,(\%) = \frac{108}{96}\Delta m\,(\%) \quad (3)$$

Where $\Delta m\,(\%)$ is the percentage of mass increase in the thermogravimetric analysis test. The measured content of active Al was 65.5% based on the test and calculation. The DSC profile of nano Al exhibits a distinct endothermic peak at 661°C, the melting endothermic peak of nano Al.

The mass of the oxidant remained unchanged. The ratio of oxidant to fuel in the thermite was allocated according to the zero oxygen balance in the chemical reaction, as shown in Table 1. Two nanothermites were prepared for comparison. In the Al/MoO_3 nanothermite, the mass of nano-MoO_3 was 120 mg. Based on the stoichiometric ratio calculation in chemical formula (4), the fuel Al required to reach zero oxygen balance for 120 mg of

MoO_3 was approximately 45 mg. However, the aluminum powder used was only 65.5% active, so the mass of the aluminum sample was 69 mg. In the Al/MoO_3/Kp nanothermite, the masses of nano-MoO_3 and Kp were 75 mg and 45 mg, respectively. Based on the calculations of the stoichiometric ratio and active Al percentage in chemical formulae (4) and (5), the required fuel Al was approximately 79 mg.

$$2Al + MoO_3 = Al_2O_3 + Mo \tag{4}$$

$$3KClO_4 + 8Al = 4Al_2O_3 + 3KCl \tag{5}$$

Nanothermite was prepared using the ultrasonic dispersion method and the preparation process is shown in Fig. 1(b). Kp was dissolved in 10 ml of DMF, heated in the water bath at 80 °C for 30 min, and labeled as solution I, where Kp exhibited a bulk-like microscopic morphology as shown in Fig. 1(b). Nano-MoO_3 and nano Al powder were dissolved in a mixture of 35 ml of DMF and 5 ml of anhydrous ethanol, magnetically stirred for 30 min, and labeled as solution II. Afterwards, the two solutions were mixed, magnetically stirred for another 30 min, and labeled as solution III. Solution III was ultrasonically dispersed for 40 min to obtain a homogeneously dispersed suspension. Finally, the suspension was dried at 80 °C for 24 h to obtain the Al/MoO_3/Kp nanothermite sample. Solution II was also ultrasonically dispersed for 40 min and dried to obtain an Al/MoO_3 nanothermite sample as the control group.

Characterization testing and thermal analysis

The sample structures were detected with X-ray diffraction (XRD, Bruker D8 Discover, Germany) at an operating voltage of 30 kV and characterized using CuKα radiation (λ=0.1542 nm) at a scan rate of 10°/min.

Scanning electron microscopy (SEM, JSM-7800 F, Japan) was used to observe the morphology of the samples. The device was used for imaging at a voltage of 5 kV and a magnification of 1?~100,000 times.

Differential scanning calorimetry (DSC, NETZSCH STA 449F3, Germany) was used to measure the thermal properties of the samples. Thermal analysis of the thermites was conducted in an argon atmosphere, with a temperature range of 40℃?~1000℃ and a heating rate of 25 K·min^{-1}. To ensure safety, the mass of the sample was 3.0 mg each time. Thermal analysis tests were performed at different heating rates of 10, 15, 20, and 25 K·min^{-1} for thermal dynamics analysis for the thermites.

Combustion test

The constant volume combustion test is shown in Fig. 2. An adjustable DC power supply was used to quickly heat a nickel-chromium wire with a diameter of 0.1 mm to ignite the thermite sample, and the experimental voltage and current were recorded using an oscilloscope (Wavesurger 3054). The closed bomb was equipped with a pressure sensor and a light intensity sensor to measure the shock wave pressure and light intensity generated by sample combustion, which was recorded with an oscilloscope. The current transfer ratio of the current detector was 1 V/A, and the relationship between pressure and voltage was P=5.63 V. To ensure safety, a small dose of thermite sample was used with a mass of 15 mg.

To observe the combustion state of thermites clearly, open combustion tests were also performed. In an open environment, the combustion process was recorded by a high-speed camera (FASTCAM SA-Z, Japan). The

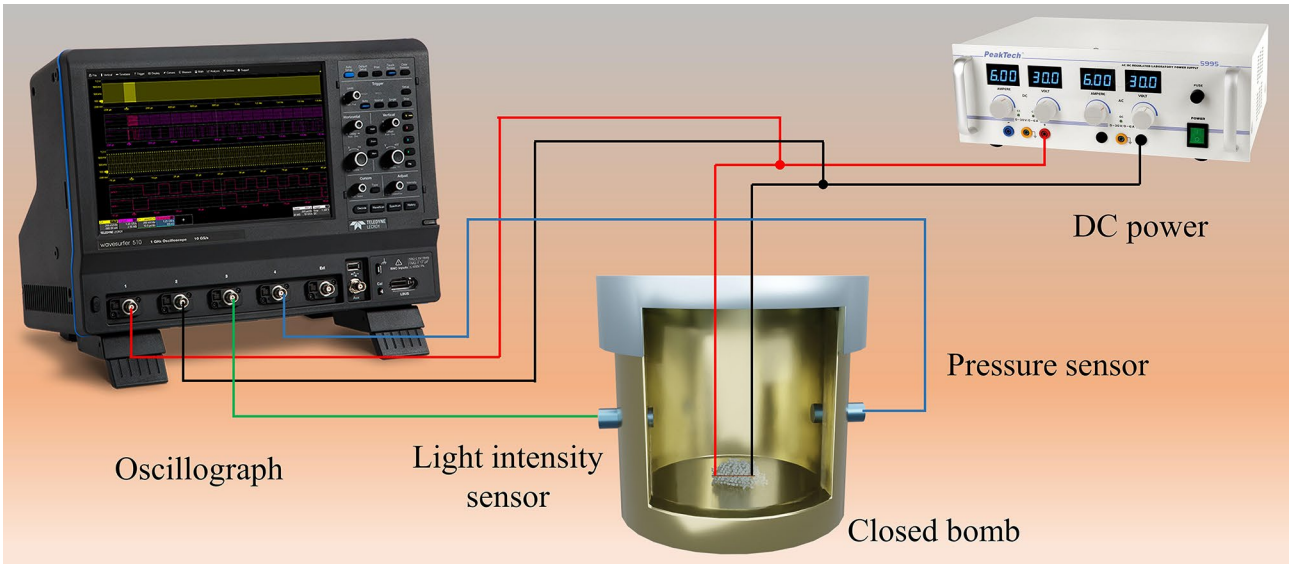

Fig. 2 Constant volume combustion test

sampling frequency was 20,000 frames per second, the frame size was 768×768 pixels, and the aperture value was 3.2. The starting point was the time when the first firelight appeared and was denoted by 0.

Results

Characterization results

Figure 3(b) is the XRD diffraction pattern of the prepared nanothermite. According to the standard comparison PDF card, as can be seen from the Fig. 3(b), the peak position and peak intensity of the Al/MoO_3 nanothermite diffraction peak match the standard phase cards MoO_3 JCPDS No.76-1003 and Al JCPDS No. 04-0787. Similarly, the peak position and peak intensity of the Al/MoO_3/Kp nanothermite diffraction peak are also consistent with the mentioned two standard cards. In addition, they are also consistent with the $KClO_4$ JCPDS No. 70–0488 standard card, which proves that the prepared nanothermite has high purity and no obvious impurities.

The microstructure of the synthesized MoO_3 is shown in the SEM image in Fig. 1(a), which exhibits a rod-shaped synthesized MoO_3, with a diameter of 80?~120 nm and a length of 15?~20 μm. Its surface is smooth and growth is regular. The microstructures of the nanothermite samples were observed using SEM, and the results are shown in Fig. 3(c)?~(h). Figure 3(c)?~(e) are the SEM and Mapping images of the Al/MoO_3 nanothermite, from which evenly distributed Al nanoparticles on the rod-shaped MoO_3 can be observed. However, there is also agglomeration of Al nanoparticles. As is well known, aluminum aggregation is inevitable, which has been reported in previous studies [36, 37]. It can be seen from the Mapping in Fig. 3(e) that Al and MoO_3 are evenly dispersed, indicating good dispersibility. In the distribution of O element, the stripes of the rod-shaped MoO_3 can be observed, and Al is distributed along the MoO_3 stripes, indicating that the Al/MoO_3 nanothermite is uniformly mixed.

Figure 3(f)?~(h) are the SEM and Mapping images of the Al/MoO_3/Kp nanothermite. The synthesized nanothermite appears to have a coating-doping shape with $KClO_4$ as its core and Al and MoO_3 as its shell. Figure 3(f)?~(g) show that Al particles and rod-shaped MoO_3 are interlaced and adhered to each other in a doped arrangement. The dense Al nanoparticles and interlaced MoO_3 have wrapped the bulk $KClO_4$. The coating structure can be further demonstrated by Fig. 3(h), where the element distribution indicates that Al is widely distributed in the periphery of the wrapped area, followed by the Mo element in the middle layer, which represents the nano-MoO_3. The K element was detected at the core, indicating a blocky $KClO_4$ core layer. They form a coating structure as shown in the diagram of the upper right corner of Fig. 3(h).

Thermal analysis results

Figure 4(a) and (b) exhibit the DSC curves of Al/MoO_3 and Al/MoO_3/Kp nanothermites at a heating rate of 25 K·min^{-1}, respectively. Over the 200?~300°C range, the DSC curves both exhibit small endothermic peaks, which is possibly due to the evaporation of adsorbed water, structured water, solvents, or impurities on the surface of the thermite during its preparation [38]. Two main exothermic peaks both appeared at approximately 500°C, which were generated from the aluminothermic reaction.

The exothermic peak of Al/MoO_3 nanothermite peaked at 568°C, as shown at the bottom-left of Fig. 4(a)

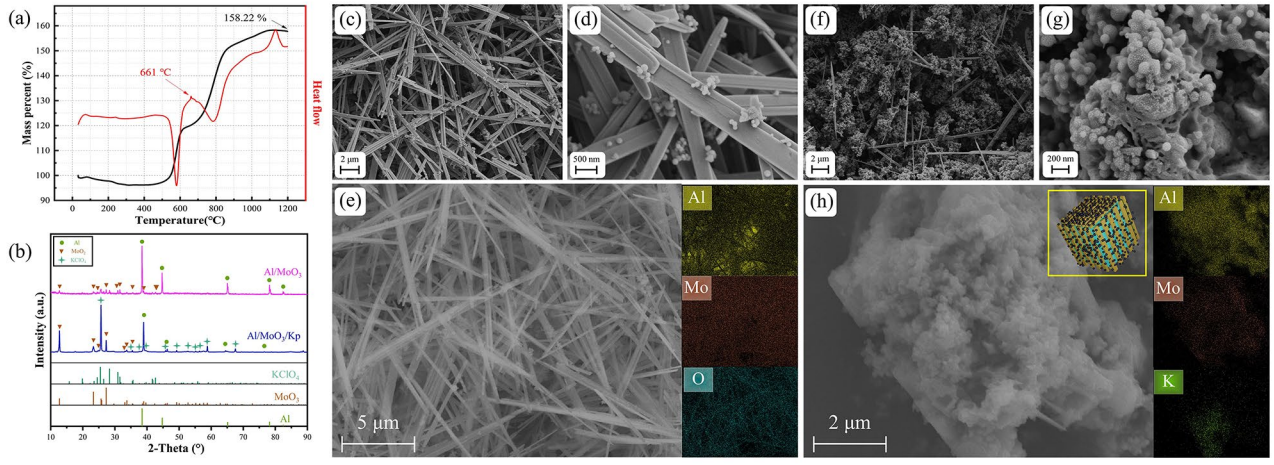

Fig. 3 Characterization diagram of the nanothermites (**a**) TG-DSC curve of nano Al heated in air (**b**) XRD diagram of the nanothermites (**c**) SEM view of the Al/MoO_3 nanothermite (**d**) Partial enlarged SEM view of the Al/MoO_3 nanothermite (**e**) Mapping image of the Al/MoO_3 nanothermite (**f**) SEM view of the Al/MoO_3/Kp nanothermite (**g**) Partial enlarged SEM view of the Al/MoO_3/Kp nanothermite (**h**) Mapping image of the Al/MoO_3/Kp nanothermite

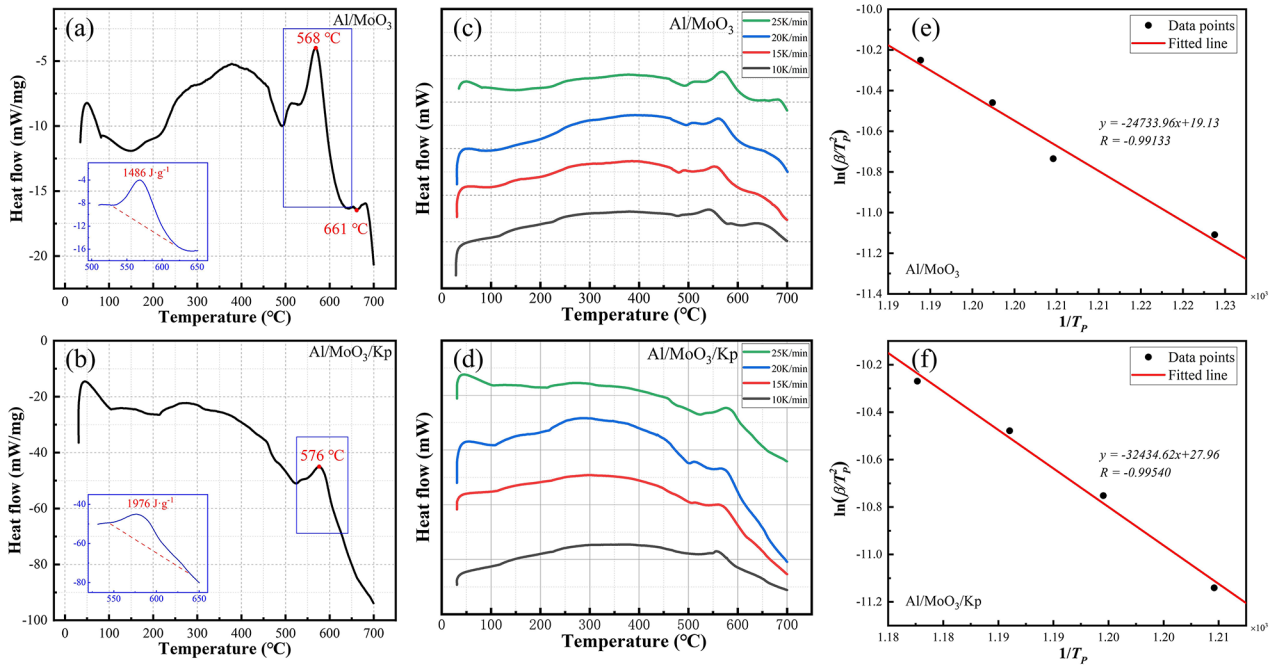

Fig. 4 DSC curves of the nanothermites. DSC curves of the nanothermites at a heating rate of 25 K·min^{-1} (**a**) Al/MoO_3, (**b**) Al/MoO_3/Kp; DSC curves of the nanothermites at different heating rates (**c**) Al/MoO_3, (**d**) Al/MoO_3/Kp; Activation energy fitting curves of the nanothermites (**e**) Al/MoO_3, (**f**) Al/MoO_3/Kp

Table 2 The main details of DSC of nanothermite

Sample	T_{onset}/°C	T_{peak}/°C	H_{exo}/J·g^{-1}
Al/MoO_3 nanothermite	539	568	1486
Al/MoO_3/Kp nanothermite	535	576	1976

Table 3 The main details of DSC curves under different heating rates

Sample	Heating rate/K·min^{-1}	T_{peak}/°C	T_{peak}/K	E_a/ kJ·mol^{-1}
Al/MoO_3 nanothermite	10	544	817	205.64
	15	557	830	
	20	562	835	
	25	568	841	
Al/MoO_3/Kp nanothermite	10	557	830	269.66
	15	564	837	
	20	570	843	
	25	576	849	

in an enlarged picture, with a total exothermic heat of 1486 J·g^{-1}, whereas the exothermic peak of Al/MoO_3/Kp nanothermite peaked at 576°C, with a total heat release of 1976 J·g^{-1}, which was approximately 33% higher than the Al/MoO_3 nanothermite, demonstrating good thermal performance. In published studies [39], the Al/Kp nanothermite, when tested using DSC, exhibited an exothermic heat release of 245.6 J·g^{-1}, which is significantly lower than that observed for the Al/MoO_3 nanothermites and the Al/MoO_3/Kp nanothermites. This comparison unequivocally demonstrates that the notable improvement in the performance of the Al/MoO_3/Kp nanothermite is primarily attributed to the catalytic promotional effect of Kp on the reaction mechanism of Al/MoO_3, rather than merely being a simple additive effect of the two reactions. Their main heat release details are listed in Table 2. It is noteworthy that there is a small endothermic peak at 661°C in the DSC curve of the Al/MoO_3 nanothermite. According to the DSC curve in Fig. 3(a), it is the melting endothermic peak of nano Al, demonstrating residual nano Al in the Al/MoO_3 nanothermite and incomplete reaction. In contrast, there is no melting endothermic peak of Al in the curve of Al/MoO_3/Kp nanothermite, wherein the nano Al had fully reacted.

Further, to investigate the thermal kinetics of the nanothermites, their activation energy (Ea) can be calculated according to the DSC curves of multiple heating rates in Fig. 4(c)?~(d).

The Kissinger [40] method was chosen to calculate the *Ea* of the thermites, as shown in Formula (6).

$$\ln\left(\frac{\beta}{T_P^2}\right) = -\frac{E_a}{RT_P} + \ln\frac{AR}{E_a} \tag{6}$$

Where A is the prefactor (s^{-1}), R is the universal gas constant (8.314 J·mol^{-1}·K^{-1}), T_P is the DSC peak temperature (K), β is the linear heating rate (K·min^{-1}). Assuming the conversion rates of the samples at the peak temperature are the same, the relationship between $ln\ (\beta/T_P^2)$ and $1/T$ is a straight line, the slope of which can be converted

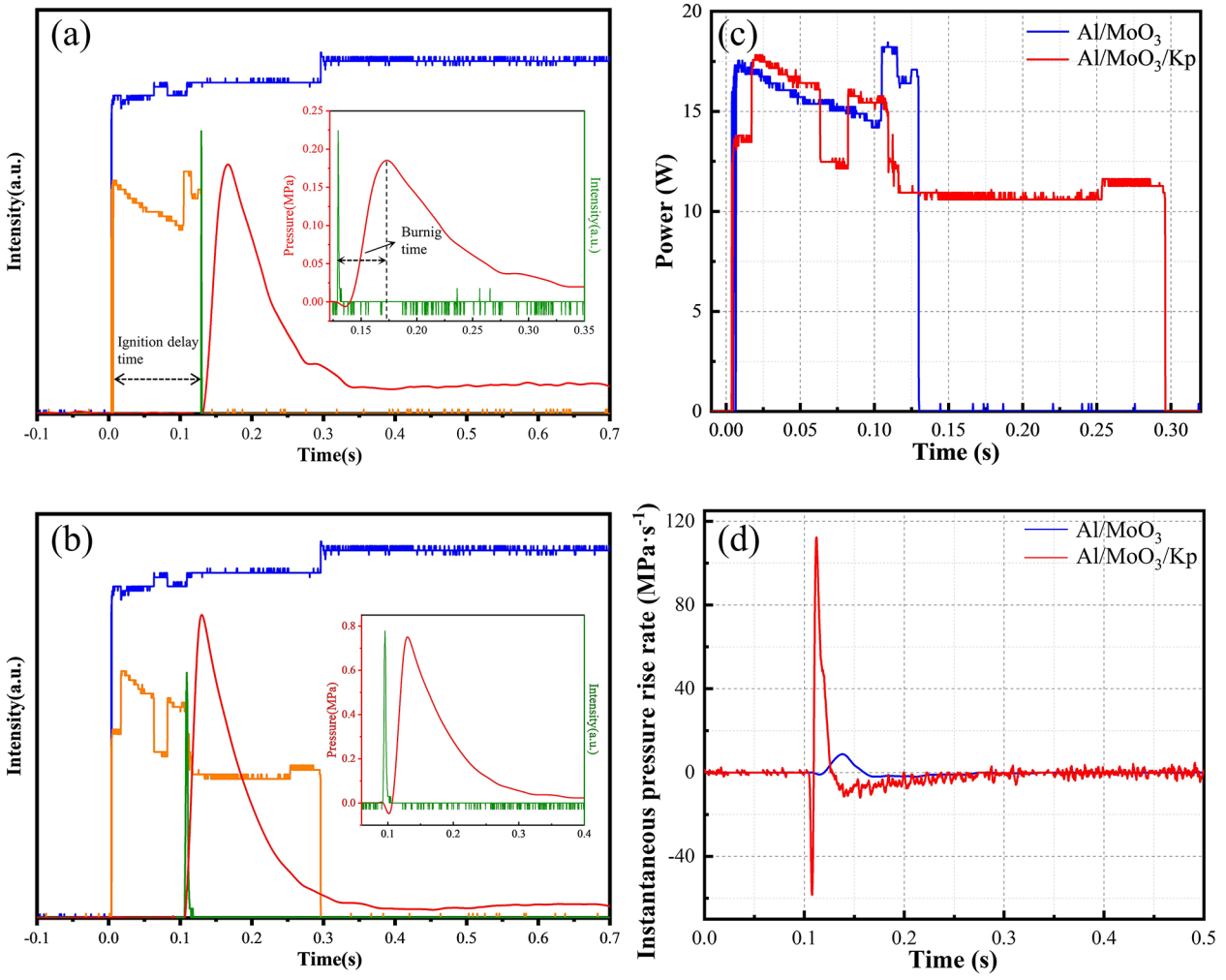

Fig. 5 Curves of the constant volume combustion tests. Combustion waveform curves: (**a**) Al/MoO_3, (**b**) Al/MoO_3/Kp; (**c**) Power-time characteristic curves of the nanothermites in the ignition delay stage (d) Instantaneous pressure rise rate curves of the nanothermites

Table 4 Detail table of combustion index of the nanothermites

Nanothermite	Ignition delay/s	Ignition energy/J	Combustion time/s	Peak pressure /MPa	Average pressure rise rate/ MPa·s^{-1}
Al/MoO_3	0.13	2.004	0.03	0.188	6.27
Al/MoO_3/Kp	0.10	1.505	0.03	0.751	25.03

into an *Ea* value, and the intercept can be converted into an *A* value.

Figure 4(c)?~(d) exhibit consistent curve trends under different heating rates, indicating good repeatability of the samples of thermal performance. The exothermic peak details of the Al/MoO_3 and Al/MoO_3/Kp nanothermites are listed in Table 3.

According to the details in Table 3, the experimental points of Al/MoO_3 and Al/MoO_3/Kp nanothermites were linearly fitted to obtain the slope equation, and then *Ea*. Figure 4(e) is the fitting result of Al/MoO_3 nanothermite. The straight line equation is *y=-24733.96x+19.13*, and the calculated Ea is 205.64 kJ·mol^{-1}. Figure 4(f) is the fitting result of Al/MoO_3/Kp nanothermite. The straight line equation *y=-32434.62x+27.96*, and the calculated *Ea* is 269.66 kJ·mol^{-1}. Activation energy is the energy required for a substance to change from a normal state to an active state that is prone to chemical reactions. The activation energy of Al/MoO_3/Kp nanothermite is higher than Al/MoO_3 by approximately 64.02 kJ·mol^{-1}, demonstrating better stability of the Al/MoO_3/Kp nanothermite.

Combustion performance

In the constant volume combustion experimental apparatus shown in Fig. 2, the oscilloscope could measure the waveform curves of the voltage (*U*) and current (*I*) flowing through the nickel-chromium wire, as well as that of the pressure (*P*) and light signal (*L*) of the nanothermite combustion. The recorded constant volume combustion

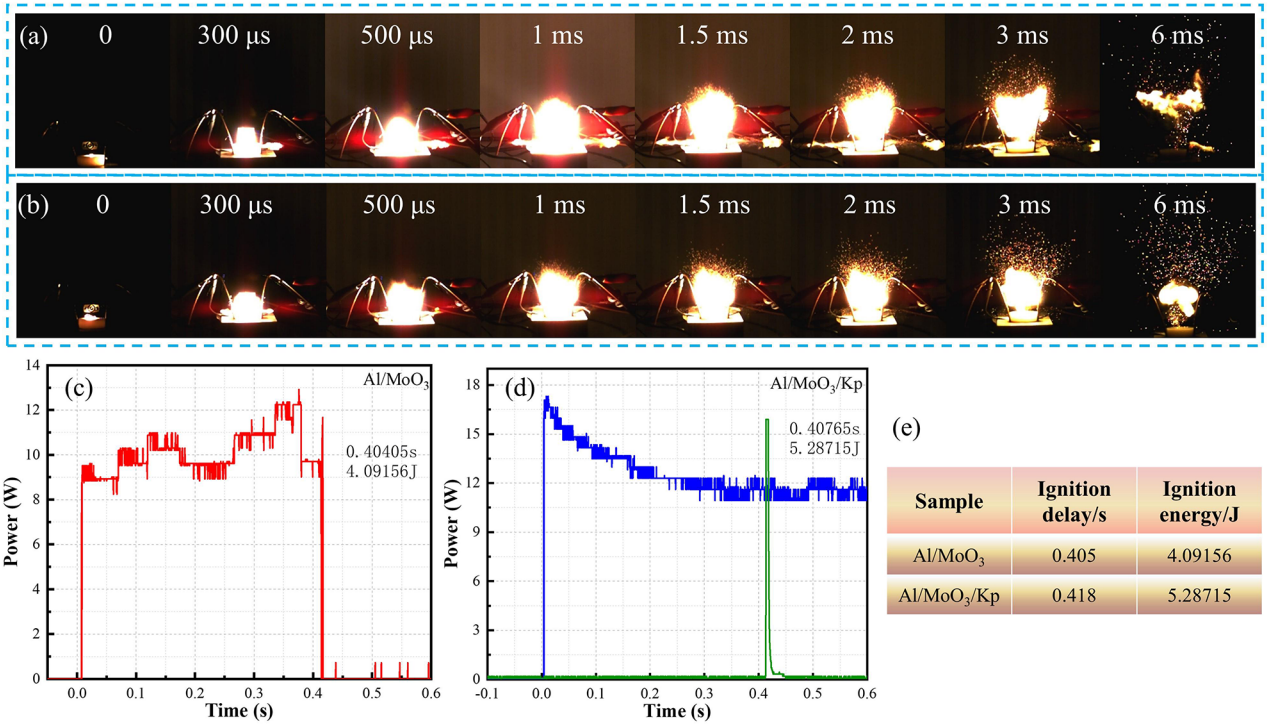

Sample	Ignition delay/s	Ignition energy/J
Al/MoO_3	0.405	4.09156
$Al/MoO_3/Kp$	0.418	5.28715

Fig. 6 Nanothermite combustion in an open environment (**a**) High speed photography of Al/MoO_3 combustion (**b**) High speed photography of $Al/MoO_3/Kp$ combustion (**c**) Power-time characteristic curve of the Al/MoO_3 nanothermite in the ignition delay stage (**d**) Power-time characteristic curve of the $Al/MoO_3/Kp$ nanothermite in the ignition delay stage (**e**) Detail table of ignition of nanothermites

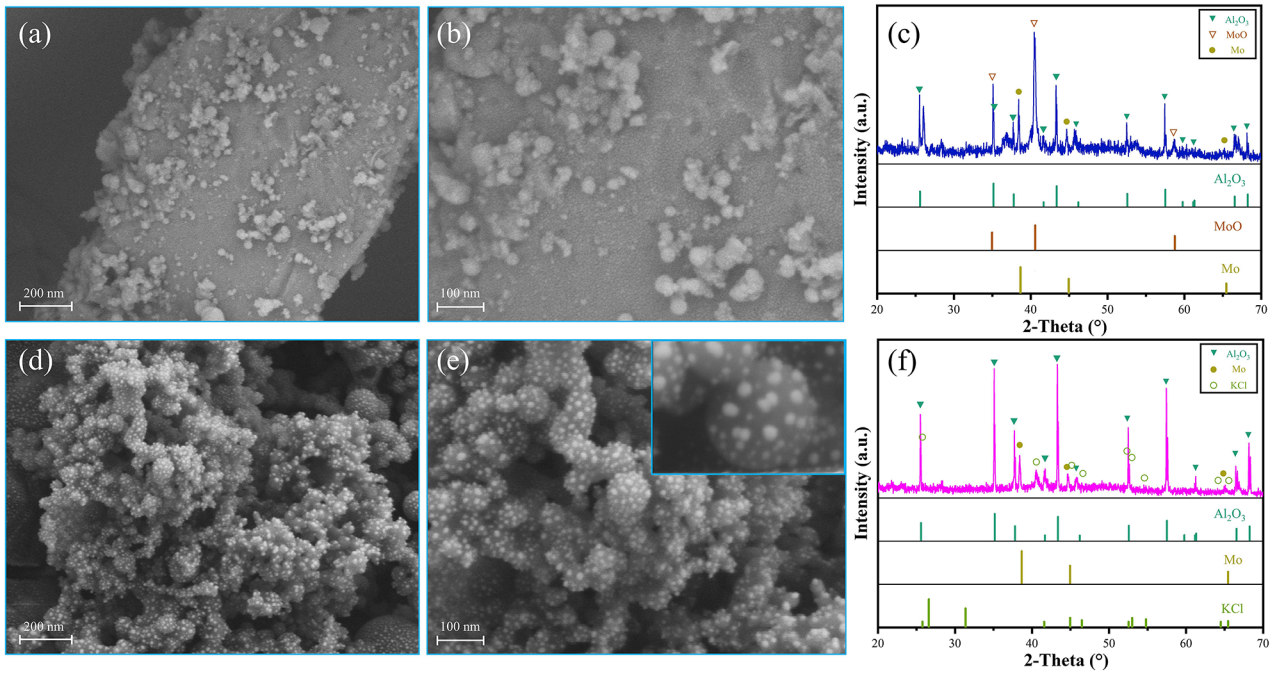

Fig. 7 Combustion product characterization diagrams of the nanothermites (**a**) SEM image of Al/MoO_3 combustion products (**b**) Locally enlarged SEM image of Al/MoO_3 combustion products (**c**) XRD patterns of Al/MoO_3 combustion products (**d**) SEM image of $Al/MoO_3/Kp$ combustion products (**e**) Locally enlarged SEM image of $Al/MoO_3/Kp$ combustion products (f) XRD patterns of $Al/MoO_3/Kp$ combustion products

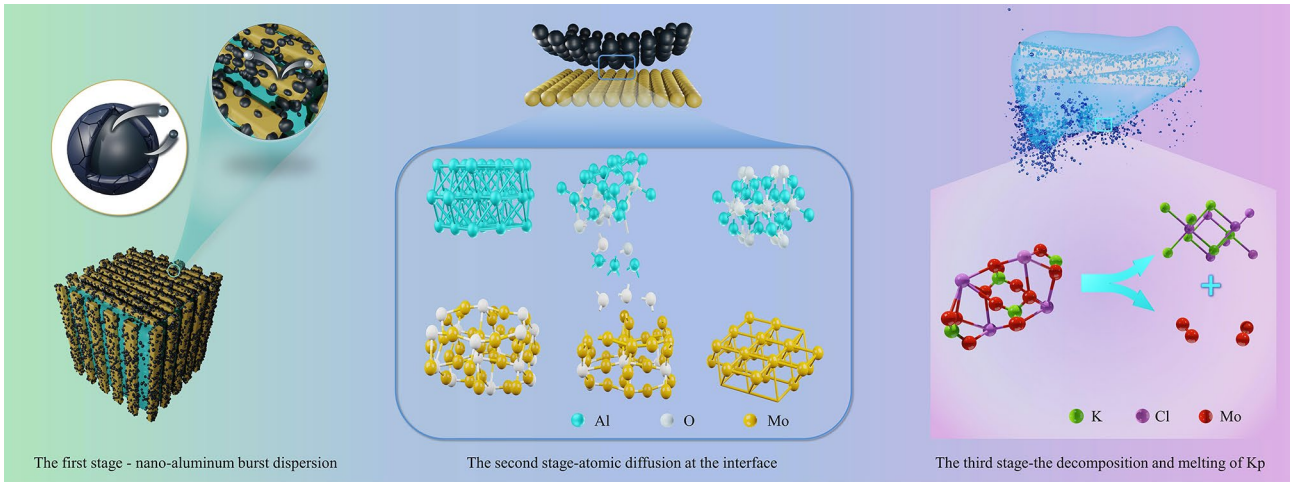

Fig. 8 Combustion mechanism diagram of the Al/MoO_3/Kp nanothermite

test waveform curves of the Al/MoO and Al/MoO_3/Kp nanothermites are shown in Fig. 5(a)?~(b).

The time between the switch closure of the constant volume combustion apparatus and the ignition of the thermite samples is defined as the ignition delay time, as shown in Fig. 5(a). The energy consumed during this period is considered to be entirely used for stimulated ignition and is defined as ignition energy. The product of voltage and current is defined as ignition power, i.e., P_{ower}=*UI*. The work done during the delay time is ignition energy, i.e., $W=\int UIdt$. The time from the generation of the light signal to the peak pressure is defined as the combustion time, as shown in Fig. 5(a). Since the pressure increased during the combustion of the thermite, when the pressure decreased, the thermite burned out. The ratio of the peak pressure to pressure rise time is defined as the average pressure rise rate. The constant volume combustion index is listed in Table 4.

The ignition performance of nanothermites reflects the degree of difficulty for them to be ignited under the action of external energy and is commonly measured by ignition temperature, ignition delay time, and ignition energy [41]. Figure 5(c) exhibits the power-time characteristic curves of the Al/MoO_3 and Al/MoO_3/Kp nanothermites in their ignition delay stage. Their instantaneous pressure rise rate curves are shown in Fig. 5(d), which are obtained by differentiating their pressure curves. After the ignition and delay time, the ignition combustion of the nanothermite samples was stimulated. The pressure in the bomb increased rapidly. The delay time of the Al/MoO_3 nanothermite was 0.13 s, ignition energy was 2.004 J, pressure peak was 0.188 MPa, combustion time was 0.03 s, and its average pressure rise rate was 6.27 MPa·s^{-1}. The delay time of the Al/MoO_3/Kp nanothermite was 0.10 s, ignition energy was 1.505 J, pressure peak was 0.751 MPa, combustion time was 0.03 s, and average pressure rise rate was 25.03 MPa·s^{-1}. The comparison reveals that the peak pressure and average pressure rise rate of the Al/MoO_3/Kp nanothermite are much higher than those of the Al/MoO_3 nanothermite, generating a large amount of gas during the reaction process, which is conducive to a faster reaction. In comparison, the Al/MoO_3/Kp nanothermite has better combustion performance than the Al/MoO_3 nanothermite. In studies detailing constant-volume combustion experiments with Al/Kp [42], the peak pressure recorded was approximately 0.214 MPa. Adding together the peak pressures for both Al/MoO_3 nanothermite and Al/Kp does not reach the peak pressure observed with the Al/MoO_3/Kp nanothermite. This evidence further highlights that the significant enhancement in the performance of the Al/MoO_3/Kp nanothermite is not merely the cumulative effect of two separate reactions. Instead, the enhancement is attributed to the catalytic promotion by Kp on the Al/MoO_3 reaction mechanism.

It is important to highlight that experimental data reveal the ignition energy needed for the Al/MoO_3/Kp nanothermite is lower compared to that of the Al/MoO_3 nanothermite. This finding may initially appear contradictory to the previously calculated activation energy, yet there is no conflict. Activation energy is the minimum energy threshold required to initiate a chemical reaction. It is a kinetic parameter that describes the energy barrier that molecules must overcome to transform from reactants to products during a chemical reaction. Ignition energy, on the other hand, typically refers to the energy that a molecule must absorb to reach an excited state from which a reaction can proceed. Typically, there is a relationship between excitation energy and activation energy, yet they operate on different orders of magnitude. Ignition energy has macroscopic characteristics, and its measured outcomes are influenced not only by

activation energy but also by changes in external environmental factors. It should be noted that the three experiments were conducted under distinct conditions. The DSC analysis took place in an environment where argon gas was continuously introduced. For the open combustion experiment, there was air circulation. Both of these experiments were affected by the gas flow rate. In contrast, the constant-volume combustion test was executed within a sealed bomb calorimeter, with static internal gases. These conditions may lead to variations in ignition energy, with the primary influences comprising: (1) Heat accumulation: Within a closed system, the challenge of dissipating heat to the environment can result in higher temperatures in the reaction zone. This temperature rise assists in reaching the critical state necessary to overcome the activation energy more rapidly, thereby enabling the reaction without the need for extra ignition energy. (2) Pressure effect: Under constant-volume sealed conditions, gases produced during the reaction increase the internal pressure of the system. This increased pressure could impact the chemical equilibrium, especially in reactions involving gaseous products. (3) Physical state transitions of substances: In conditions of high temperature and/or pressure, reactants or catalysts might experience phase changes, such as transitioning from solid to liquid, potentially altering the reaction pathway. (4) Impact of environmental conditions: Within the constraints of a constant-volume sealed system, the exchange of heat and matter with the external environment is restricted. This limitation may induce alterations in the microenvironment of the reactants, including fluctuations in local temperatures and pressures, each of which could potentially influence ignition energy required.

To acquire a clearer combustion morphology of the nanothermites, the closed bomb was removed and the combustion process was captured using high-speed photography. The test was a constant pressure combustion one because it was performed in an open environment. The combustion morphology captured by high-speed photography is shown in Fig. 6(a)?~(b), with the recording time of the initial combustion image as the starting point, which is recorded as time 0.

The two thermites had similar combustion morphology and reaction time, and both reached the most intense moment of combustion at approximately 1 ms, accompanied by bright light and explosion sound. Since the constant pressure combustion took place in an open environment and was not subjected to any constraints, it went rapidly. The thermites almost burned out within 6 ms. However, their combustion processes were partially different.

Unlike the Al/MoO_3 nanothermite, the combustion of Al/MoO_3/Kp nanothermite was accompanied by sparks spattering, proving that a large amount of gas was produced during the process, which was also confirmed in the constant volume combustion test. Moreover, The ignition delay time and energy of the Al/MoO_3 and Al/MoO_3/Kp nanothermites were slightly different, as shown in Fig. 6(c)?~(e). The ignition delay time of Al/MoO_3/Kp nanothermite is slightly longer, and its ignition energy is higher than that of the Al/MoO_3 nanothermite. Therefore, the combustion of Al/MoO_3/Kp nanothermite requires more energy and has a certain stability. The results are consistent with the activation energy analysis.

Characterization of combustion products

Figure 7 exhibit the SEM electron micrographs and XRD images of the combustion products of the nanothermites. Figure 7(a)?~(b) show the microscopic SEM images of the combustion products of Al/MoO_3 nanothermite, exhibiting small particles uniformly adhered to the nano-rod. XRD detection, as shown in Fig. 7(c), reveals that the products comprise Al_2O_3 (JCPDS No.74-1081), MoO (JCPDS No.78–0424), and Mo (JCPDS No.88-2331). This result indicates that the aluminothermic reaction occurred during the combustion process of Al/MoO_3 nanothermite, whereas MoO_3 was not completely reduced, and this reaction was not complete. Based on the SEM image, it could be speculated that the rod was the produced Mo and the incompletely reduced MoO.

The combustion products of Al/MoO_3/Kp nanothermite resemble a dense "coral", as shown in Fig. 7(d)?~(e). This is possibly the effect of reactants melt and then solidification during the combustion process. The enlarged view of a sphere in Fig. 7(e) shows many white dots adhering to its surface. These white dots evenly cover the entire "coral-like" surface. Figure 7(f) is the XRD pattern of the combustion products of Al/MoO_3/Kp, which comprise Al_2O_3, Mo, and KCl. Previous studies have found that the melting and thermal decomposition temperature for $KClO_4$ is approximately 570°C [30, 43, 44], at which it decomposes into KCl and O_2. The generation of a large amount of O_2 gas is consistent with the results in the constant volume tests. The melting point of KCl is approximately 770°C [20, 45]. During the combustion process, the temperature is high enough to reach this melting point. Therefore, the "coral-like" product forms by solidifying after melting. From the obtained experimental results, it can be deduced that the observed molten "coral-like" formations are composed of KCl. The produced Mo appears to have undergone melt blending with the KCl. The white dot-like substances observed on the outer surface have been identified as Al_2O_3.

Discussion

The excellent thermal and combustion performance of Al/MoO_3/Kp nanothermite is closely related to its distinctive reaction mechanism. During the rapid heating

process, Al/MoO_3/Kp nanothermite mainly undergoes three stages of reaction, and its main reaction mechanism is shown in Fig. 8.

The first stage is the burst diffusion stage of nano Al from the oxide layer. In the published literature, there are three prevailing views on the diffusion mechanism of nano Al covered with an oxide layer: diffusion-oxidation mechanism [46, 47], ion diffusion mechanism [48], and melting-diffusion mechanism [49, 50].

The diffusion-oxidation mechanism is that when the heating rate is low, the pressure gradient affects the diffusion of the central Al, i.e., when nano Al is oxidized, the Al atoms in the nucleus diffuse outward and the oxygen atoms diffuse inward [51, 52]. The ion diffusion mechanism suggests that the ignition of Al nanoparticles covered with an oxide layer is mainly due to the internal electric field generated by the alumina layer on the surface, which accelerates the diffusion rate of Al ions through the oxide layer and enhances their diffusion strength. This Intrinsic electric field drives approximately 90% of Al ion mass through [48, 53]. The melting-diffusion mechanism refers to the phenomenon where at extremely high heating rates, the volume of the nucleus expands, the pressure increases, the oxide layer splits, and the liquid-phase aluminum disperses into small liquid-phase clusters that fly off at high speeds [54–56]. The combustion test was realized by rapid heating with an electric current, so the ion diffusion mechanism and melting-diffusion mechanism might occur. According to the SEM images of the combustion products in Fig. 7(a)?~(b), it can be inferred that nano Al droplets must have splashed during the combustion process. Therefore, the melting-diffusion mechanism was more likely to occur.

The combustion of nanothermite was rapidly heated by electric current to stimulate the reaction. In the process of continuous conversion of electric energy into thermal energy, the temperature in the thermite increased continuously, which made the nano Al covered with an alumina protective layer burst and disperse out of the layer. The nano Al droplets dropped on the reactants, allowing the nano Al to come into close contact with the reactants, as shown in the first stage of Fig. 8.

The second stage is the atomic diffusion behavior at the interface between nano Al and the oxidant, i.e., the rapid redox reaction dominated by the metal-oxygen flipping mechanism at the interface [55]. In this stage, the Al atoms in nano Al and O atoms in MoO_3 diffused with each other and rapidly combined to form Al-O bonds [57]. Since the reaction occurred at the interface, nano Al was extremely close to the reactants, resulting in a fast reaction rate, as shown in the second stage of Fig. 8.

The third stage is the most important. The published studies have all concluded that this stage is a slow reaction dominated by atomic diffusion motion, which is mainly due to the long mass transfer distance, thus resulting in low reaction efficiency. In the Al/MoO_3/Kp nanothermite, the rapid melt and decomposition of Kp enables the reaction to proceed efficiently.

It is well known that increasing the contact area between the reactants or the pressure can significantly improve reaction efficiency. A large number of studies have shown that the melting and low-temperature thermal decomposition temperature of $KClO_4$ is about 570 °C [30, 43, 44], where it changes frome solid to liquid and decomposes into KCl and O_2. The peak of the aluminothermic reaction at the interface is about 576 °C (Fig. 4 (b)). At this time, Kp rapidly melts and decomposes into KCl and O_2. On the one hand, Kp melted into liquid and wrapped Al and MoO_3 tightly, making the contact between the reactants closer and accelerating the reaction; on the other hand, Kp continuously decomposed into O_2, leading to an increase in local pressure, which rapidly increased the pressure in the constant volume combustion test (Fig. 5(b)). Simultaneously, splashing sparks could be seen in the combustion morphology (Fig. 6(b)). Moreover, O_2 provided an oxidizing agent, which promoted the reaction, increased the reaction efficiency, greatly improved the reaction rate of the third stage, and even converted the third stage into the reaction at the interface, which greatly improved the efficiency of the aluminothermic reaction. It could be inferred from the combustion products that all reactants were completely reacted, demonstrating excellent combustion performance. When the reaction was completed, the reactants exhibited a unique morphology of "coral-like" (Fig. 7(e)).

In the case of Al/MoO_3 nanothermite, after the nano Al burst and dispersed out of the protective layer in the first stage, the second stage of the reaction occurred at the interface between Al and MoO_3, however, in the third stage, the reaction did not fully proceed due to discontinuous reaction medium or excessively sparse nano Al droplets, resulting in an incomplete reduction of MoO_3 and the presence of MoO in the combustion products.

In the DSC test, nano Al tended to diffuse from the protective layer through the diffusion-oxidation mechanism due to the slow heating. Afterwards, similar to the combustion reaction, the melt and decomposition of Kp increased the contact area between the reactants. O_2 was produced to provide an oxidant, which increased the internal pressure of the reactants and promoted the progress of the reaction, facilitating the complete reaction between reactants. Therefore, a large amount of heat was released, demonstrating good thermal performance.

Conclusions

In this study, the Al/MoO_3/Kp and Al/MoO_3 nanothermites were prepared using the ultrasonic dispersion method. Then the prepared nanothermites were tested for their thermal and combustion properties. Thermomechanical analysis was conducted, and the reaction mechanism of Al/MoO_3/Kp nanothermite was investigated.

The three main stages of the Al/MoO_3/Kp nanothermite reaction were the bursting reaction where nano Al underwent melt and diffusion, the atomic diffusion at the interface between the reactants, and the rapid melt and decomposition of Kp. The distinctive third stage was the key to excellent thermal and combustion properties. The reactants were melted and wrapped and O_2 was produced to increase pressure, thus the aluminothermic reaction was promoted comprehensively, leading to a heat release of 1976 $J{\cdot}g^{-1}$, a combustion peak pressure of 0.751 MPa, and an extremely fast average pressure rise rate of 25.03 $MPa{\cdot}s^{-1}$. Its performance is much better than Al/MoO_3 nanothermite, the control group. Moreover, the Ea of Al/MoO_3/Kp nanothermite is 269.66 $kJ{\cdot}mol^{-1}$, which is more stable and safer than the 205.64 $kJ{\cdot}mol^{-1}$ of Al/MoO_3 nanothermite. The strategy of altering the physical states of reactants during the reaction process, though demanding precise manipulation and high-accuracy equipment, offers crucial insights for the development of novel, superior performance nanothermites. This innovative approach is informative and holds significant potential for the advancement of nanothermite performance.

Author contributions

J.C., S.L. and M.D. designed the experiments; R.S., Y.C. and Q.Y. performed material preparation, data collection and analysis; J.C., S.L., M.A. performed the experiments and analyzed the data; J.S., Q.T. and X.Z. contributed reagents/materials/analysis tools and participated in the data discussion; all authors participated in the analysis, interpretation, and review of the results and provided input in the writing process of the paper.

Funding

This research was funded by Qin Chuangyuan talent project in Shanxi Province, grant number No. QCYRCXM-2022-274.

Data availability

All data generated or analyzed during this study are included in this article. The data that support the findings of this study are available from the corresponding author, [author initials], upon reasonable request.

Declarations

Ethics approval and consent to participate

Not applicable.

Consent for publication

Not applicable.

Competing interests

The authors declare no competing interests.

Received: 1 February 2024 / Accepted: 22 April 2024
Published online: 09 May 2024

References

1. Zhang ZH, Shen Y, Wang CA, Wang YT, Li FW, Cheng J, et al. An excellent synergy between CL-20 and nanothermites in flaming and propelling with high specific impulse and superior safety to electrostatic discharge. Combust Flame. 2022;240:112024.
2. Wang YT, Li FW, Shen Y, Wang CA, Zhang ZH, Xu JB, et al. Fabrication of high electrostatic safety metastable Al/CuO nanocomposites doped with nitro-functionalized graphene with fast initiation ability and tunable reaction performance. Combust Flame. 2021;233:111580.
3. Wang QH, Ma YC, Wang YL, Bao HB, Li AQ, Xu P, et al. Facile fabrication of highly exothermic CuO@Al nanothermites via self-assembly approach. Nanotechnology. 2020;31(5):055601.
4. Zhang C, Mao H, Cui R, Zhang X, Yang J, Ji J, et al. Electrospinning preparation, energetic characteristics and reaction mechanism of corrosion-resistant Si@PVDF nanostructured energetic films. Combust Flame. 2022;237:111887.
5. Qin Y, Yu HM, Wang DQ, Song Y, Li FS, Liu J. Preparation and characterization of energetic composite films with mutual reactions based on B/PVDF mosaic structure. Chem Eng J. 2023;451:138792.
6. Yang H, Xu C, Man S, Bao H, Xie Y, Li X, et al. Effects of hollow carbon nanospheres on combustion performance of Al/Fe_2O_3-based nanothermite sticks. J Alloys Compd. 2022;918:165684.
7. Song JX, Guo T, Ding W, Yao M, Yang L, Zhang XN, et al. The Effect of Al particles size on the Thermal Behavior and kinetics of Al-MnO_2 Thermite System. Adv Mater Sci Eng. 2020;2020:3097404.
8. Wang ST, Zhang YG, Ma XC, Wang WZ, Li XB, Zhang ZD, et al. Hydrothermal route to single crystalline alpha-MoO_3 nanobelts and hierarchical structures. Solid State Commun. 2005;136(5):283–7.
9. Sui HT, Li BY, Wen JZ. Interaction between single-walled Carbon nanotubes and reactive nanoparticle constituents in multilayered Al/NiO Nanocomposite. ACS Appl Energy Mater. 2018;1(10):5245–56.
10. Grobler JM, Focke WW, Derrick NP, Oberholster AJ, Kelly C, Labuschagne G. Sensitising the micron-sized aluminium/potassium periodate thermite. J Energ Mater. 2020;38(4):455–66.
11. Delgado A, Cordova S, Shafirovich E. Thermite reactions with oxides of iron and silicon during combustion of magnesium with lunar and martian regolith simulants. Combust Flame. 2015;162(9):3333–40.
12. Wang JJ, Guo ZQ, Chen SH, Zhang WZ, Cui H, Qin Z, et al. Self-assembly preparation of advanced metastable MCo_2O_4/GO/Al (M = cu, mg, Zn, Ni) nanothermites to realize large heat release, stable combustion and high safety. Ceram Int. 2022;48(14):20825–37.
13. Yang H, Yang G, Li X, Bao H, Yang Y, Guo X, et al. Facile synthesis of high tightly ordered Al/CuO core-shell nanowire arrays and the effect of surface density on combustion. J Alloys Compd. 2021;877:160025.
14. de Castro IA, Datta RS, Ou JZ, Castellanos-Gomez A, Sriram S, Daeneke T, et al. Molybdenum Oxides - from fundamentals to Functionality. Adv Mater (Weinheim Germany). 2017;29(40):1701619.
15. Wang JB, Li HL, Hu CY, Wang ZY, Han K, Liu D, et al. The efficiency of Thermite-assisted underwater Wet Flux-Cored Arc Welding process: electrical dependence, Microstructural Changes, and Mechanical properties. Metals. 2023;13(5):831.
16. Yang HF, Xu CH, Wang WM, Tang PF, Li XD, He SS, et al. Underwater self-sustaining combustion and micro-propulsion properties of Al@FAS-17/PTFE-based direct-writing nanothermite. Chem Eng J. 2023;451:138720.
17. Huang C, Chen J, Bai S, Li S, Tang Y, Liu X, et al. Enhancement of energy release performance of Al–Ni composites by adding CuO. J Alloys Compd. 2020;835:155271.
18. Hu XL, Xiao LQ, Jian XX, Zhou WL. Integration of nano-Al with one-step synthesis of MoO_3 nanobelts to realize high exothermic nanothermite. Sci Eng Compos Mater. 2018;25(3):579–85.
19. Yu CP, Zhang WC, Gao Y, Ni DB, Ye JH, Zhu CG, et al. The super-hydrophobic thermite film of the Co_3O_4/Al core/shell nanowires for an underwater ignition with a favorable aging-resistance. Chem Eng J. 2018;338:99–106.
20. Liu PA, Wang MJ, Wang L, Wang J, Wang T. Study on Nano-Metal Oxide and Carbon Nanotube composites on Thermal decomposition of Potassium Perchlorate. Bull Korean Chem Soc. 2019;40(4):324–31.
21. Wang HY, Jian GQ, Egan GC, Zachariah MR. Assembly and reactive properties of Al/CuO based nanothermite microparticles. Combust Flame. 2014;161(8):2203–8.
22. Jacob RJ, Jian GQ, Guerieri PM, Zachariah MR. Energy release pathways in nanothermites follow through the condensed state. Combust Flame. 2015;162(1):258–64.

23. Wang Y, Song XL, Jiang W, Deng GD, Guo XD, Liu HY, et al. Mechanism for thermite reactions of aluminum/iron-oxide nanocomposites based on residue analysis. Trans Nonferrous Met Soc China. 2014;24(1):263–70.
24. Chen JH, Ren W, Hu B, Zheng ZL, Chen YJ, Chen JH, et al. Effect of the Ni and NiO Interface Layer on the Energy Performance of Core/Shell CuO/Al Systems. Langmuir. 2020;36(43):12858–65.
25. Chen JL, Guo T, Ding W, Song JX, Yao M, Bei FL, et al. Effect of CuO on the thermal kinetics and combustion properties of Al/MoO_3 thermite prepared by ball milling. Ceram Int. 2021;47(12):16500–10.
26. Zhou X, Xu DG, Yang GC, Zhang QB, Shen JP, Lu J, et al. Highly exothermic and Superhydrophobic Mg/Fluorocarbon Core/Shell Nanoenergetic Arrays. ACS Appl Mater Interfaces. 2014;6(13):10497–505.
27. Wang QH, Yang SB, Bao HB, Wang QY, Li XM, Yang WJ. Self-assembled core-shell structured Si@CuO energetic materials for enhanced exothermic performance. Vacuum. 2019;169:108881.
28. Yan S, Jian GQ, Zachariah MR. Electrospun Nanofiber-based Thermite textiles and their reactive properties. ACS Appl Mater Interfaces. 2012;4(12):6432–5.
29. Wu CW, Sullivan K, Chowdhury S, Jian GQ, Zhou L, Zachariah MR. Encapsulation of Perchlorate salts within Metal Oxides for Application as Nanoenergetic Oxidizers. Adv Funct Mater. 2012;22(1):78–85.
30. Yang F, Kang XL, Luo JS, Yi Z, Tang YJ. Preparation of core-shell structure $KClO_4$@Al/CuO nanoenergetic material and enhancement of thermal behavior. Sci Rep. 2017;7:3730.
31. Zhou X, Wang YJ, Cheng ZP, Ke X, Jiang W. Facile preparation and energetic characteristics of core-shell Al/CuO metastable intermolecular composite thin film on a silicon substrate. Chem Eng J. 2017;328:585–90.
32. Zhou X, Xu DG, Lu J, Zhang KL. CuO/Mg/fluorocarbon sandwich-structure superhydrophobic nanoenergetic composite with anti-humidity property. Chem Eng J. 2015;266:163–70.
33. Kang XL, Li CH, Zheng Z, Cui XD. Synthesis of ZnO and Cu-doped ZnO Nanocrystalline by Solution Combustion Method and their Catalytic effects on Thermal Behavior of $KClO_4$. Combust Sci Technol. 2021;193(1):75–89.
34. Gao K, Li GP, Luo YJ, Wang L, Shen LH, Wang G. Preparation and characterization of the AP/Al/Fe_2O_3 ternary nano-thermites. J Therm Anal Calorim. 2014;118(1):43–9.
35. Zhou X, Zhu Y, Ke X, Zhang KL. Exploring the solid-state interfacial reaction of Al/Fe_2O_3 nanothermites by thermal analysis. J Mater Sci Lett. 2019;54(5):4115–23.
36. Wang L, Yan DR, Dong YC, Zhang JX, Chen XG. Nanostructured ceramic composite coating prepared by reactive plasma spraying micro-sized Al-Fe_2O_3 composite powders. Ceram Int. 2013;39(3):2437–42.
37. Song JX, Guo T, Ding W, Yao M, Bei FL, Zhang XN, et al. Study on thermal behavior and kinetics of Al/MnO_2 poly(vinylidene fluorine) energetic nanocomposite assembled by electrospray. RSC Adv. 2019;9(44):25266–73.
38. Dose WM, Donne SW. Manganese dioxide structural effects on its thermal decomposition. Mater Sci Eng B-Advanced Funct Solid-State Mater. 2011;176(15):1169–77.
39. Kang X, Li C, Zheng Z, Cui X. Synthesis of ZnO and Cu-doped ZnO Nanocrystalline by Solution Combustion Method and their Catalytic effects on Thermal Behavior of $KClO_4$. Combust Sci Technol. 2021;193(1):75–89.
40. Kissinger HE. Reaction kinetics in differential thermal analysis. Anal Chem. 1957;29(11):1702–6.
41. Song JX, Guo T, Yao M, Chen JL, Ding W, Zhang XN, et al. Hindering effect of graphene oxide on reaction performance of Al/MnO_2 nanothermite system. Colloid Interface Sci Commun. 2020;37:100271.
42. Zhou W, DeLisio JB, Wang X, Zachariah MR. Reaction mechanisms of potassium oxysalts based energetic composites. Combust Flame. 2017;177:1–9.
43. Fathollahi M, Behnejad H. A comparative study of thermal behaviors and kinetics analysis of the pyrotechnic compositions containing mg and Al. J Therm Anal Calorim. 2015;120(2):1483–92.
44. Ba SH, Zhang Z, Yan MH, Sun ZX, Teng XP. Effect of Nano-CuO on luminous intensity of Pyrotechnics Composite containing $KClO_4$ and al. Advanced materials and process technology2012. p. 669–72.
45. Liu PA, Wang MJ, Wang L, Wang J, Wang T. Effect of nano-metal oxide and nano-metal oxide/graphene composites on thermal decomposition of potassium perchlorate. Chem Pap. 2019;73(6):1489–97.
46. Park K, Lee D, Rai A, Mukherjee D, Zachariah MR. Size-resolved kinetic measurements of aluminum nanoparticle oxidation with single particle mass spectrometry. J Phys Chem B. 2005;109(15):7290–9.
47. Rai A, Park K, Zhou L, Zachariah MR. Understanding the mechanism of aluminium nanoparticle oxidation. Combust Theor Model. 2006;10(5):843–59.
48. Henz BJ, Hawa T, Zachariah MR. On the role of built-in electric fields on the ignition of oxide coated nanoaluminum: ion mobility versus fickian diffusion. J Appl Phys. 2010;107(2):024901.
49. Levitas VI, Asay BW, Son SF, Pantoya M. Mechanochemical mechanism for fast reaction of metastable intermolecular composites based on dispersion of liquid metal. J Appl Phys. 2007;101(8):083524.
50. Levitas VI, Pantoya ML, Dean S. Melt dispersion mechanism for fast reaction of aluminum nano- and micron-scale particles: Flame propagation and SEM studies. Combust Flame. 2014;161(6):1668–77.
51. Zhao Y, Mei Z, Zhao FQ, Xu SY, Ju XH. Atomic perspectives revealing the evolution behavior of aluminum nanoparticles in energetic materials. Appl Surf Sci. 2021;563:150296.
52. Chu QZ, Shi BL, Liao LJ, Luo KH, Wang NF, Huang CG. Ignition and Oxidation of Core-Shell Al/Al_2O_3 nanoparticles in an Oxygen Atmosphere: insights from Molecular Dynamics Simulation. J Phys Chem C. 2018;122(51):29620–7.
53. Zhdanov VP, Kasemo B. Cabrera-Mott kinetics of oxidation of nm-sized metal particles. Chem Phys Lett. 2008;452(4–6):285–8.
54. Zhong K, Niu LL, Li G, Zhang CY. Crack mechanism of Al@Al_2O_3 nanoparticles in hot energetic materials. J Phys Chem C. 2021;125(4):2770–8.
55. Zhang JP, Si YB, Leng C, Yang BC. Molecular dynamics simulation of Al-SiO_2 sandwich nanostructure melting and low-temperature energetic reaction behavior. RSC Adv. 2016;6(64):59313–8.
56. Hao WZ, Li G, Niu LL, Gou RJ, Zhang CY. Molecular Dynamics Insight into the evolution of Al Nanoparticles in the Thermal decomposition of energetic materials. J Phys Chem C. 2020;124(19):10783–92.
57. Zhu ZY, Ma B, Tang CM, Cheng XL. Molecular dynamic simulation of thermite reaction of Al nanosphere/Fe_2O_3 nanotube. Phys Lett A. 2016;380(1–2):194–9.

Publisher's Note